INTERNATIONAL JOURNAL FOR NUMERICAL METHODS IN FLUIDS
Int. J. Numer. Meth. Fluids 2008; **57**:811–838
Published online 15 November 2007 in Wiley InterScience (www.interscience.wiley.com). DOI: 10.1002/fld.1646

Third-order Cartesian overset mesh adaptation method for solving steady compressible flows

O. Saunier[1,‡], C. Benoit[1,*,†,‡], G. Jeanfaivre[1,‡] and A. Lerat[2,§]

[1]*ONERA, Châtillon, France*
[2]*ENSAM, Paris, France*

SUMMARY

A third-order mesh generation and adaptation method is presented for solving the steady compressible Euler equations. For interior points, a third-order scheme is used on Cartesian and curvilinear meshes. Concerning the mesh adaptation, the method of Meakin is also extended to third order. The accuracy of the new overset mesh adaptation method is demonstrated by a grid convergence study for 2-D inviscid model problems and results are compared with a second-order method. Finally, the method is applied to the computation of an inviscid 3-D flow around a hovering blade of the ONERA 7A helicopter rotor exhibiting an improvement in the wake capture. With a 7 million point mesh, the tip vortex can be followed for more than three rotor revolutions with the third-order method. The CPU time needed for this calculation is only 3% higher than with a conventional second-order method. Copyright © 2007 John Wiley & Sons, Ltd.

Received 8 June 2007; Revised 21 September 2007; Accepted 25 September 2007

KEY WORDS: third-order scheme; mesh adaptation; chimera method; finite-volume method; Euler equations; helicopter rotor

1. INTRODUCTION

The chimera method is a domain decomposition approach using overset body conforming grids. In this approach, each component of a configuration is meshed separately and overset onto a background grid to form the complete computational domain. This method introduced in 1983 by Steger *et al*. [1] has become popular to compute flows around complex geometries. However, the required number of points for an accurate capture of complex flows can become high very quickly. To overcome this difficulty, Meakin [2] proposed a mesh adaptative refinement method within

*Correspondence to: C. Benoit, ONERA, Châtillon, France.
†E-mail: christophe.benoit@onera.fr
‡Research Scientist.
§Professor.

systems of overset Cartesian grids. This method has been developed by Benoit and Jeanfaivre [3] and successfully applied to the capture of the vortical wake of helicopter rotors in hovering flight by solving the Euler equations using the Jameson, Schmidt and Turkel [4] (JST) scheme. The first interest of the automatic approach of Meakin is to simplify the mesh generation process. As a matter of fact, generating structured grids with no constraints on the outer boundary is far simpler than multi-block structured mesh generation. Other interests inherent to the use of Cartesian grids are that they have a simpler and faster solver, do not require the metric storage and enable high-order numerical schemes to be simply written.

The purpose of the present study is to improve this mesh adaptation method by increasing the order of accuracy of the numerical scheme. Numerous works have been devoted to high-order schemes for the Euler or Navier–Stokes equations (see, for instance, the recent survey lectures in Reference [5]). Here, we have chosen to keep close to the JST scheme frequently used in industrial codes and to consider the third-order extension of this scheme proposed by Cinnella and Lerat [6] and Cinnella *et al.* [7]. This finite-volume scheme is third-order accurate on moderately deformed grids and at least second-order accurate on highly deformed grids. Recent studies have shown that it is possible to extend these high-order numerical schemes to overset-grid topologies [8]. Nevertheless, linear interpolation is unable to keep the global accuracy of an overset-grid method [9] and consequently the use of high-order interpolation is required.

In this paper, we first recall in Section 2 the third-order finite-volume scheme on curvilinear meshes and its finite difference version on Cartesian grids. In Section 3, we briefly recall the basic mesh adaptation technique; then we describe the new developments.

The accuracy of the transfers of numerical solution between Cartesian grids is increased by using Lagrange interpolation. In Section 4, the improvements to the initial method are illustrated for a steady vortex, a subsonic flow past a NACA0012 airfoil, then the third-order method is applied to an inviscid 3-D flow field around a hovering blade of the 7A helicopter rotor.

2. THIRD-ORDER SCHEME FOR INTERIOR POINTS

For interior points, we use the numerical scheme of Cinnella and Lerat [6] and Cinnella *et al.* [7] which is third-order accurate, even on curvilinear meshes. Let us recall the main features of this scheme in two space dimensions. We first present the finite-volume formulation on a general structured mesh, introduce the numerical flux and the treatment of the volume integral term; then we present the formulation of this scheme on a Cartesian mesh and finally the numerical dissipation.

2.1. Numerical flux

Consider the 2-D hyperbolic system of conservation laws expressed in integral form as

$$\frac{\mathrm{d}}{\mathrm{d}t}\int_{\Omega} w\,\mathrm{d}\Omega+\int_{\partial\Omega} F(w)\cdot n\,\mathrm{d}\Gamma=0 \tag{1}$$

where Ω is a bounded domain with boundary $\partial\Omega$, n is the unit outward normal to $\partial\Omega$ and $F(w)=[f(w), g(w)]$ is the flux density.

For the Euler equations

$$w_t+f(w)_x+g(w)_y=0 \tag{2}$$

DOI: 10.1002/fld

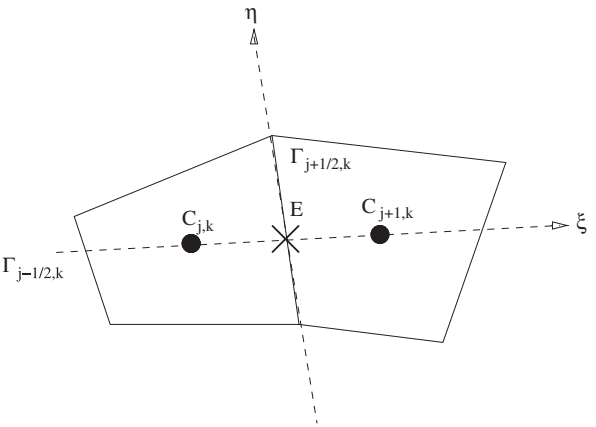

Figure 1. Definitions for mesh cells.

with

$$w=\begin{pmatrix}\rho\\ \rho u\\ \rho v\\ \rho E\end{pmatrix},\quad f(w)=\begin{pmatrix}\rho u\\ \rho u^2+p\\ \rho uv\\ \rho uH\end{pmatrix},\quad g(w)=\begin{pmatrix}\rho v\\ \rho uv\\ \rho v^2+p\\ \rho vH\end{pmatrix} \tag{3}$$

where ρ is the density, p the pressure, u and v the Cartesian components of the fluid velocity, E is the specific total energy and $H=E+p/\rho$ is the specific total enthalpy with, for a perfect gas

$$p=(\gamma-1)\rho\left(E-\frac{u^2+v^2}{2}\right) \tag{4}$$

Define a structured mesh composed of quadrangular cells $\Omega_{j,k}$ (see Figure 1) and denote the cell centers by $C_{j,k}$, and the cell edges by $\Gamma_{j+1/2,k}$ or $\Gamma_{j,k+1/2}$:

$$\partial\Omega_{j,k}=\{\Gamma_{j+1/2,k},\ \Gamma_{j,k+1/2},\ \Gamma_{j-1/2,k},\ \Gamma_{j,k-1/2}\} \tag{5}$$

Applied to the cell $\Omega_{j,k}$, the conservation laws (1) become

$$\frac{\mathrm{d}}{\mathrm{d}t}\int_{\Omega_{j,k}} w\,\mathrm{d}\Omega+\sum_{\Gamma\in\partial\Omega_{j,k}}\int_{\Gamma}F(w)\cdot n\,\mathrm{d}\Gamma=0 \tag{6}$$

The numerical flux density $F_{j+1/2,k}$ through the edge $\Gamma_{j+1/2,k}$ of the cell $\Omega_{j,k}$ is an approximation to

$$\frac{1}{|\Gamma_{j+1/2,k}|}\int_{\Gamma_{j+1/2,k}}F(w)\cdot n\,\mathrm{d}\Gamma \tag{7}$$

To define a local reference frame on the edge $\Gamma_{j+1/2,k}$, let ξ be an axis passing through the adjoining cell center, oriented from $C_{j,k}$ to $C_{j+1,k}$ and let η be an axis on $\Gamma_{j+1/2,k}$. Let E be the intersection point of the η and ξ axes.

DOI: 10.1002/fld

Performing a Taylor expansion in the η-direction, we obtain the following third-order approximation of the exact flux:

$$\frac{1}{|\Gamma_{j+1/2,k}|}\int_{\Gamma_{j+1/2,k}} F(w)\cdot n\,\mathrm{d}\Gamma=(\phi+\beta_1\phi_\eta+\beta_2\phi_{\eta\eta})_{|E}+O(h^3) \tag{8}$$

with $\phi=Fn$ and

$$\beta_1=\frac{\int_\Gamma(\eta-\eta_{|E})\,\mathrm{d}\eta}{|\Gamma_{j+1/2,k}|}=O(h) \tag{9}$$

$$\beta_2=\frac{\int_\Gamma(\eta-\eta_{|E})^2\,\mathrm{d}\eta}{2|\Gamma_{j+1/2,k}|}=O(h^2) \tag{10}$$

where $\eta|_E$ is the coordinate of E on the η-axis ($\eta_{|E}=0$) and $h=|C_{j,k}C_{j+1,k}|$.

In formula (8), $\phi_{|E}$, $\phi_{\eta|E}$ and $\phi_{\eta\eta|E}$ are, respectively, discretized to the third-, second- and first-order accuracy. This is done in a centered way by using weighted average and difference operators taking into account the locations of E and of the surrounding cell centers. Third-order approximation of $\phi_{|E}$ is obtained by cancelling the error term introduced by weighted average which discretizes $\phi_{|E}$ to second-order accuracy. Numerical flux is third-order accurate [7] on moderately deformed meshes and at least second-order accurate on highly distorted meshes.

If the grid deformations were neglected, the above weighted numerical flux would be reduced to

$$F_{j+1/2,k}=(\mu_1\phi-\tfrac{1}{8}\delta_1^2\mu_1\phi+\tfrac{1}{24}\delta_2^2\mu_1\phi)_{j+1/2,k} \tag{11}$$

where δ_1, δ_2, μ_1 and μ_2 denote the following discrete operators:

$$\begin{aligned}&(\delta_1 u)_{j+1/2,k}=u_{j+1,k}-u_{j,k},\quad (\delta_2 u)_{j,k+1/2}=u_{j,k+1}-u_{j,k}\\&(\mu_1 u)_{j+1/2,k}=\tfrac{1}{2}(u_{j+1,k}+u_{j,k}),\quad (\mu_2 u)_{j,k+1/2}=\tfrac{1}{2}(u_{j,k+1}+u_{j,k})\end{aligned} \tag{12}$$

We will see later the improvements brought by the weighted formula (8).

2.2. Volume integral

For steady problems, which are our main concern in the present study, it is sufficient to approximate the volume integral in the unsteady term of (1) by the simplest formula:

$$\frac{\mathrm{d}}{\mathrm{d}t}\int_{\Omega_{j,k}} w\,\mathrm{d}\Omega=|\Omega_{j,k}|w_{t|j,k}+O(h^2) \tag{13}$$

where $w_{t|j,k}$ is the time derivative of w at the cell center of $\Omega_{j,k}$ and $|\Omega_{j,k}|$ is the cell area.

However, this volume integral term must be approximated to third-order accuracy in the general case. This can be achieved on a general structured mesh [10]. Nevertheless, for the sake of simplicity, we limit the presentation to the case of a regular Cartesian grid.

Denoting the space steps by δx and δy—of the same order, say $O(h)$—the volume integral can be expanded as

$$(UT)_{j,k}=\frac{\mathrm{d}}{\mathrm{d}t}\int_{\Omega_{j,k}} w\,\mathrm{d}\Omega=\delta x\delta y\left(w_t+\frac{\delta x^2}{24}w_{txx}+\frac{\delta y^2}{24}w_{tyy}\right)_{j,k}+O(h^4) \tag{14}$$

DOI: 10.1002/fld

Using the local form of the conservation laws

$$w_t = -f_x - g_y \tag{15}$$

the unsteady term becomes

$$\frac{1}{\delta x \delta y}(UT)_{j,k} = (w_t)_{j,k} - \frac{\delta x^2}{24}(f_{xxx} + g_{xxy})_{j,k} - \frac{\delta y^2}{24}(f_{xyy} + g_{yyy})_{j,k} + O(h^4) \tag{16}$$

Using the above discrete operators δ_1, δ_2, μ_1 and μ_2, a fourth-order approximation of the unsteady term is

$$\frac{1}{\delta x \delta y}(\widetilde{UT})_{j,k} = (w_t)_{j,k} - \frac{1}{24}\left(\frac{\delta_1^3 \mu_1 f}{\delta x} + \frac{\delta_1^2 \delta_2 \mu_2 g}{\delta y} + \frac{\delta_1 \mu_1 \delta_2^2 f}{\delta x} + \frac{\delta_2^3 \mu_2 g}{\delta y}\right)_{j,k} \tag{17}$$

which can also be expressed as

$$\frac{1}{\delta x \delta y}(\widetilde{UT})_{j,k} = (w_t)_{j,k} - \frac{1}{24}\left[\frac{\delta_1}{\delta x}(\delta_1^2 + \delta_2^2)\mu_1 f\right]_{j,k} - \frac{1}{24}\left[\frac{\delta_2}{\delta y}(\delta_1^2 + \delta_2^2)\mu_2 g\right]_{j,k} \tag{18}$$

The time derivative has also to be accurately approximated. For an unsteady problem, a classical explicit third-order Runge–Kutta method is used. For a steady problem, an implicit method based on the first-order backward Euler method is chosen to get a quick convergence to the steady state and is efficiently solved using a LU relaxation algorithm [11]. The semi-discrete schemes corresponding to the weighted flux (8) and the non-weighted flux (11) with a third-order approximation of volume integral are, respectively, called FVW-3 and FV-3 schemes.

2.3. Formulation of the scheme on a regular Cartesian mesh

Let us express the complete scheme for computing unsteady flows on a regular Cartesian grid, since this type of grid is our main concern in our mesh adaptation technique. Here, we combine the fourth-order accurate volume integral term (18) with the numerical flux which reduces to (11) with $\phi = f$ on $\Gamma_{j+1/2,k}$ and $\phi = g$ on $\Gamma_{j,k+1/2}$, that is

$$\begin{aligned} F_{j+1/2,k} &= [(I - \tfrac{1}{8}\delta_1^2 + \tfrac{1}{24}\delta_2^2)\mu_1 f]_{j+1/2,k} \\ F_{j,k+1/2} &= [(I - \tfrac{1}{8}\delta_2^2 + \tfrac{1}{24}\delta_1^2)\mu_2 g]_{j,k+1/2} \end{aligned} \tag{19}$$

The finite-volume scheme becomes

$$\frac{1}{\delta x \delta y}(UT)_{j,k} + \left(\frac{\delta_1 F}{\delta x}\right)_{j,k} + \left(\frac{\delta_2 F}{\delta y}\right)_{j,k} = 0 \tag{20}$$

and can be rewritten in the very simple form as

$$\left[w_t + \frac{\delta_1}{\delta x}\left(I - \frac{1}{6}\delta_1^2\right)\mu_1 f + \frac{\delta_2}{\delta y}\left(I - \frac{1}{6}\delta_2^2\right)\mu_2 g\right]_{j,k} = 0 \tag{21}$$

This Cartesian scheme is purely directional, i.e. it involves points only in the x and y directions passing through the cell center $C_{j,k}$. This formulation of the third order of numerical scheme on

DOI: 10.1002/fld

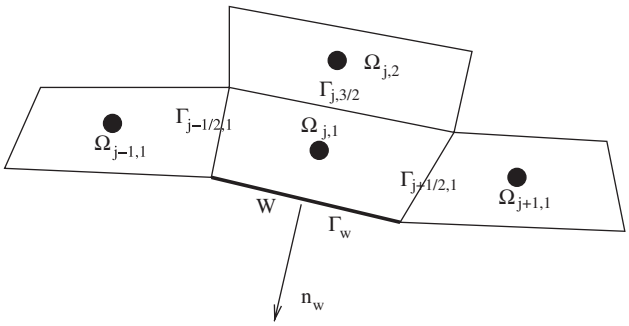

Figure 2. Mesh cells around a wall.

regular Cartesian grids, which can be seen as a finite difference formulation, is strictly equivalent to the finite-volume approach. Expression (21) is much simpler than the general finite-volume formula and will be implemented this way on the Cartesian grids of the mesh adaptation method for efficiency reasons. This specific formulation on Cartesian grids is called DNC.

2.4. Numerical dissipation

To ensure numerical stability and avoid spurious oscillations, a numerical dissipation is added to the present third-order method. For simplicity, we use the Jameson artificial dissipation [4]. For instance, for the Cartesian scheme, this leads to the modification of the numerical fluxes in the j direction (with similar modification in the k direction) as follows:

$$F_{j+1/2,k} = (F - D)_{j+1/2,k} \tag{22}$$

with the dissipation

$$(D)_{j+1/2,k} = \rho(\overline{A}_{j+1/2,k})(\varepsilon_2 \delta_1 w - \varepsilon_4 \delta_1^3 w)_{j+1/2,k} \tag{23}$$

where $\overline{A}_{j+1/2,k}$ is an average of the Jacobian matrix $A = \mathrm{d}f/\mathrm{d}w$, $\rho(A)$ denotes the spectral radius of matrix A and

$$\varepsilon_{2|j+1/2,k} = k_2 \max(v_{j,k}, v_{j+1,k}), \quad \varepsilon_{4|j+\frac{1}{2},k} = \max(0, k_4 - \varepsilon_{2|j+1/2,k}) \tag{24}$$

$$v_{j,k} = \frac{|p_{j+1,k} - 2p_{j,k} + p_{j-1,k}|}{|p_{j+1,k} + 2p_{j,k} + p_{j-1,k}|} \tag{25}$$

where p is the static pressure and k_2, k_4 are constant parameters. In a region where w is smooth, $\varepsilon_2 = O(h^2)$ and $\varepsilon_4 = O(1)$, so that the dissipative terms are $O(h^3)$ and the whole scheme remains third-order accurate.

2.5. Wall slip boundary condition

Consider a mesh cell $\Omega_{j,k}$ adjacent to a rigid wall W and denote by n_W the normal to the edge $\Gamma_{j,1/2} = \Gamma_W$ located on the wall (see Figure 2). The boundary of $\Omega_{j,1}$ is made of four edges:

$$\partial\Omega_{j,1} = \{\Gamma_W,\ \Gamma_{j,3/2},\ \Gamma_{j+1/2,1},\ \Gamma_{j-1/2,1}\} \tag{26}$$

DOI: 10.1002/fld

By multiplying the momentum equation in the cell $\Omega_{j,1}$ by the wall normal n_W, we obtain the normal momentum equation:

$$\frac{\mathrm{d}}{\mathrm{d}t}\int_{\Omega_{j,1}} \rho n_W \cdot V \,\mathrm{d}\Omega + \int_{\partial\Omega_{j,1}} [\rho n_W \cdot V(V\cdot n) + p n_W \cdot n]\,\mathrm{d}\Gamma = 0 \tag{27}$$

where $V=(u, v)$ is the fluid velocity. On the edge Γ_W, $n=n_W$ and due to the slip condition

$$(V\cdot n)_W = 0 \tag{28}$$

so that the wall momentum flux reduces to

$$\int_{\Gamma_W} p \,\mathrm{d}\Gamma \tag{29}$$

The time derivative of the normal momentum in $\Omega_{j,1}$—i.e. the first integral in (27)—vanishes at a steady state. In the transient phase, the slip condition yields that this integral remains small. By neglecting it, we compute the normal flux from (27) as

$$\int_{\Gamma_W} p \,\mathrm{d}\Gamma = -\int_{\Gamma_{j,3/2},\ \Gamma_{j+1/2,1},\ \Gamma_{j-1/2,1}} [\rho n_W \cdot V(V\cdot n) + p n_W \cdot n]\,\mathrm{d}\Gamma \tag{30}$$

where the fluxes in the right-hand side are obtained through centered formulae. This gives the pressure p_W on the edge Γ_W:

$$p_W = -n_W \frac{1}{(\delta\Gamma)_W}[(\mu_1 \overline{\phi}\delta\Gamma)_{j+1/2,1} + (\mu_1 \overline{\phi}\delta\Gamma)_{j-1/2,1} + (\mu_2 \overline{\phi}\delta\Gamma)_{j,3/2}] \tag{31}$$

where $\delta\Gamma$ denotes an edge length and

$$\overline{\phi} = \begin{pmatrix} F^{(2)}(w)\cdot n \\ F^{(3)}(w)\cdot n \end{pmatrix} \tag{32}$$

$F^{(2)}$ and $F^{(3)}$ being the second and the third lines, respectively, of the flux density in (1)

$$F^{(2)} = [\rho u^2 + p,\ \rho u v], \quad F^{(3)} = [\rho u v,\ \rho v^2 + p] \tag{33}$$

Practically, the conservative variables in the cell $\Omega_{j,1}$ are advanced at time $(n+1)\Delta t$ using the numerical scheme, except for the edge Γ_W, where the flux is obtained from p_W given by (31) at time $n\Delta t$.

3. THIRD-ORDER MESH ADAPTATION METHOD

In the mesh adaptation method [2, 3] studied in this paper, short curvilinear grids (called 'body' grids) are defined around the bodies and the complete computational domain is discretized by automatically generated and adapted Cartesian grids. These Cartesian grids are adapted following a refinement indicator, based on the numerical solution and computed on the mesh. The mesh adapted to the refinement indicator is obtained by determining homogeneous clusters in the refinement field. For this purpose, the algorithm makes use of a dichotomic/fusion approach. Then, on each

DOI: 10.1002/fld

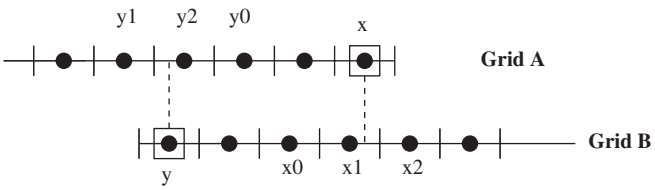

Figure 3. Interpolated points for third-order chimera.

cluster a uniform Cartesian grid is generated. The number of points after a remeshing is controlled by a growing factor defined by the user.

Communication transfers between curvilinear and Cartesian grids are ensured through the chimera method. In the chimera method, mesh points are classified into three categories: 'hole' points, 'interpolated' points and 'interior' points. Hole points lie physically inside a body and are consequently not computed, interpolated points are evaluated by interpolation of the flow field of another grid and 'interior' points are updated through the interior numerical scheme. For an interpolated point, Lagrange polynomials are used in the case of transfer between Cartesian grids and triangular or tetrahedral linear interpolation is applied in the case of transfer between a body grid and a Cartesian grid.

In our previous version of the method, the numerical scheme for interior points was the classical finite-volume JST scheme [4] and the mesh adaptation method was also second-order accurate.

3.1. Third-order interpolation

After having increased the order of accuracy of the interior numerical scheme, the order of accuracy of chimera transfers must also be increased. This is realized for interpolations between Cartesian grids by using directional Lagrange polynomials. Let $n+1$ distinct interpolation points x_j, $j=0,\ldots,n$, be given, together with corresponding set of values f_j. Let $\prod_n$ denote the vector space of all polynomials of degree at most n. The classical problem addressed here is to find the polynomial $p\in\prod_n$ that interpolates f at the points x_j, i.e.

$$p(x_j)=f_j, \quad j=0,\ldots,n \tag{34}$$

The problem is well posed, i.e. it has a unique solution that depends continuously on the data. The solution can be expressed in Lagrange form as

$$p(x)=\sum_{j=0}^{n} f_j l_j(x), \quad l_j(x)=\frac{\prod_{k=0,k\neq j}^{n}(x-x_k)}{\prod_{k=0,k\neq j}^{n}(x_j-x_k)} \tag{35}$$

The Lagrange polynomial l_j corresponding to the node x_j has the property

$$l_j(x_k)=\begin{cases}1, & j=k\\ 0 & \text{otherwise}\end{cases} \tag{36}$$

In this work, n is chosen equal to 2. Consider the interpolation in one-space direction between two grids A and B (see Figure 3). Let x a point to be interpolated on the grid A (see Figure 3) and $\delta x=|x_{i+1}-x_i|$, $i>0$.

DOI: 10.1002/fld

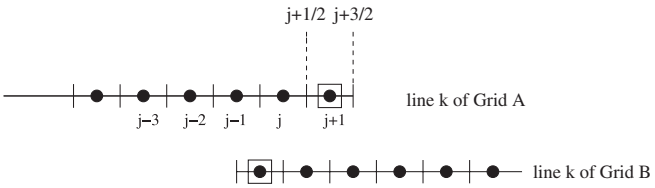

Figure 4. Minimum overlap with one layer of interpolated cells.

The third point x_0 on grid B is chosen such as

$$\begin{cases} x_0 = x_1 - \delta x & \text{if } |x - x_1| < \dfrac{\delta x}{2} \\ x_0 = x_2 + \delta x & \text{otherwise} \end{cases} \tag{37}$$

3.2. Modification of numerical flux for one layer of interpolation cells

In the chimera method, the number of grid points in the overlap region has to be sufficient to ensure a proper communication between the grids: an interpolated point must be computed from 'interior' points. If a valid interpolation cell cannot be found, the interpolated point is called an orphan point. Instead of finding a proper treatment for orphan points, an alternative procedure is to avoid their occurrence. For this purpose, only one layer of interpolated cell is chosen, even for a 5-point scheme in 1-D as proposed in Reference [12]. Of course, numerical fluxes have to be modified for the interfaces near interpolated points, if possible, without loss of accuracy.

Let us examine the situation of Figure 4. The values on the last cell face $(j+\frac{3}{2},k)$ of grid A are always interpolable, otherwise grid B would be too small and thus useless. Consequently, the values on the last cell face are computed by Lagrange interpolation. The interior cell faces can be computed by the current formula until the face $(j-\frac{1}{2},k)$. For the last interior face $(j+\frac{1}{2},k)$, we now present a technique to obtain the physical flux and the artificial viscosity flux with the desired third-order accuracy without additional interpolation.

3.2.1. Physical flux on the last interior face. We recall that the interior numerical flux without dissipation in direction j is given by the following formula:

$$F_{j+1/2,k} = (\mu_1 f - \tfrac{1}{6}\delta_1^2 \mu_1 f)_{j+1/2,k} \tag{38}$$

In the case of overset between two Cartesian grids along the direction j and if we consider only one layer of interpolation cells, the approximation of $F_{j+1/2,k}$ must be modified. This is realized by using a non-centered discretization that allows to preserve the third-order accuracy on the derivative f. For one layer of interpolation cells, flux at $(j+\frac{1}{2},k)$ is given by

$$F_{j+1/2,k} = \tfrac{1}{12}(2f_{j+1,k} + 17f_{j,k} - 11f_{j-1,k} + 5f_{j-2,k} - f_{j-3,k}) \tag{39}$$

For a regular curvilinear mesh, we have chosen to modify the flux from the non-weighted version of $F_{j+1/2,k}$ given by

$$F_{j+1/2,k} = (\mu_1 \phi - \tfrac{1}{8}\delta_1^2 \mu_1 \phi + \tfrac{1}{24}\delta_2^2 \mu_1 \phi)_{j+1/2,k} \tag{40}$$

DOI: 10.1002/fld

By using a non-centered approximation this flux becomes

$$F_{j+1/2,k}=\tfrac{1}{16}(9\phi_{j,k}+8\phi_{j+1,k}-\phi_{j-1,k}-\delta_1\phi_{j+3/2,k})+\tfrac{1}{24}\delta_2^2\mu_1\phi_{j+1/2,k} \tag{41}$$

with $\delta_1\phi_{j+3/2,k}$ defined by the second-order non-centered approximation:

$$\delta_1\phi_{j+3/2,k}=\tfrac{8}{3}\phi_{j+3/2,k}+\tfrac{1}{3}\phi_{j,k}-3\phi_{j+1,k} \tag{42}$$

3.2.2. Artificial viscosity flux on the last interior face. First of all, the sensor v given by (25) is modified in the last cell. It is estimated by using a second-order approximation for the second derivative:

$$v_{j+1,k}=\frac{|2p_{j,k}+\frac{16}{5}p_{j+3/2,k}-\frac{1}{5}p_{j-1,k}-5p_{j+1,k}|}{|2p_{j,k}+\frac{16}{5}p_{j+3/2,k}+\frac{1}{5}p_{j-1,k}+5p_{j+1,k}|} \tag{43}$$

The first-order difference involved in the artificial viscosity is computable as usual. For the third-order difference of a scalar field w in point $(j+\frac{1}{2},k)$, a non-centered second-order accurate formula is used:

$$\delta w_{j+3/2,k}=\tfrac{8}{3}w_{j+3/2,k}+\tfrac{1}{3}w_{j,k}-3w_{j+1,k} \tag{44}$$

4. NUMERICAL ASSESSMENT OF ACCURACY

In this section, the actual orders of accuracy of JST method and of the third-order method are evaluated from a steady vortex test case on single block Cartesian and curvilinear meshes. Then, the computations are performed on overlapping meshes to show the importance of the order of accuracy of interpolations. The coupling between the third-order scheme and mesh adaptation method is performed for a subsonic flow past an NACA0012 airfoil. The order of accuracy is determined by grid convergence for each computation. Finally, the third-order method is applied to the computation of an inviscid flow around a hovering helicopter blade and results are compared with the second-order method.

4.1. Steady vortex

We consider the 2-D inviscid vortex proposed by Yee *et al.* [13] for which the entropy is uniform. The vortex is located at the origin ($x=y=0$) in a flow at rest. Its velocity components u, v and the absolute temperature T are defined in non-dimensional form as

$$\begin{aligned}(u,v)&=\frac{\Gamma}{2\pi}\mathrm{e}^{(1-r^2)/2}(-y,x)\\ T&=-\frac{(\gamma-1)\Gamma^2}{8\gamma\pi^2}\mathrm{e}^{1-r^2}\end{aligned} \tag{45}$$

where $r^2=x^2+y^2$. The vortex strength Γ is set equal to $\Gamma=5$ and the specific heat ratio is $\gamma=1.4$. The uniformity of entropy gives $\rho=T^{1/(\gamma-1)}$. This vortex is a steady solution of the Euler equations using the above vortex as the initial condition and periodic boundary conditions. The observed evolution is uniquely due to the numerical errors. The objective is to assess the real order

DOI: 10.1002/fld

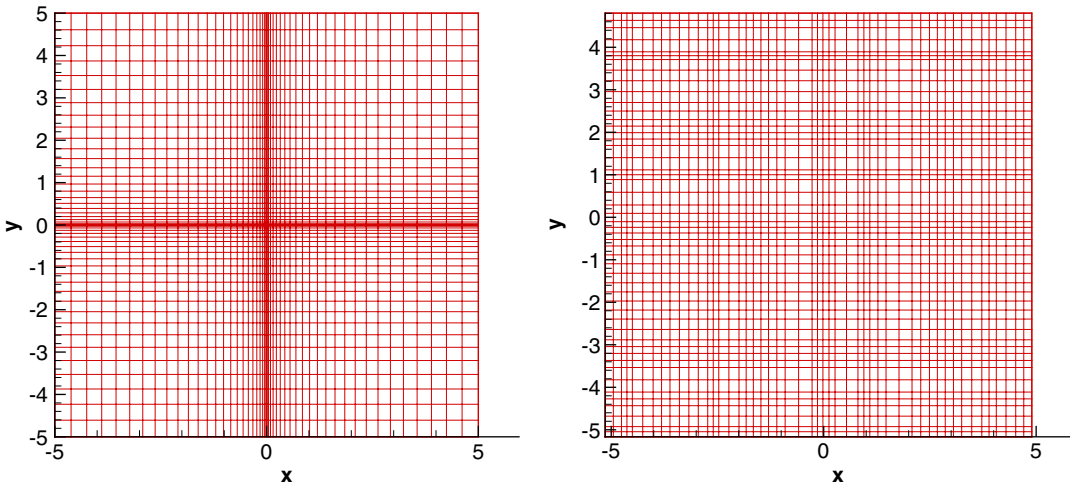

Figure 5. View of stretched and randomized Cartesian grids—Yee vortex.

Table I. Order of accuracy of different schemes on Cartesian meshes—Yee vortex.

	Cartesian meshes		
Scheme	Uniform	Stretched	Irregular
JST	2	1.93	1.1
JSTW	2	1.9	1.75
DNC	3	xx	xx
FV-3	3	2.34	1.1
FVW-3	3	3	2.5

of accuracy of DNC (Cartesian mesh version), FV-3 (non-weighted version for a general mesh) and FVW-3 (weighted version) schemes in comparison with the original JST scheme.

4.1.1. Single block meshes. All computations are performed on the domain $[-5,5]\times[-5,5]$. In a first step, three kinds of Cartesian grids are used: uniform, stretched and randomized grids (Figure 5). In each case, the numerical error is evaluated using three grids of increasing refinement corresponding to $\delta x = 0.4$, 0.2 and 0.1 in the uniform grid case. The computed flow density is compared with the exact density distribution. For these calculations, a weighted version of the classical JST scheme has been developed, it will be called JSTW scheme. In order to realize this extension, the technique is the one described in Section 2.2 but with a numerical flux of second-order accuracy. On the other hand, on regular Cartesian grids, FVW-3 and FV-3 schemes are obviously identical to DNC formulation.

JST and JSTW schemes have been coupled with the second-order accurate four-stage Runge–Kutta explicit [4] method and DNC, FV-3 and FVW-3 schemes have been used with an explicit third-order Runge–Kutta method. Besides, in order to minimize the influence of the time discretization, the numerical solution is computed only at time $t = 0.1$ and time steps are 0.1, 0.05 and 0.025 on

DOI: 10.1002/fld

Table II. Order of accuracy of different schemes on curvilinear meshes—Yee vortex.

	Curvilinear meshes	
Scheme	Regular	Irregular
JST	1.96	0.83
JSTW	2.03	1.87
FV-3	2.72	1.03
FVW-3	2.74	2.4

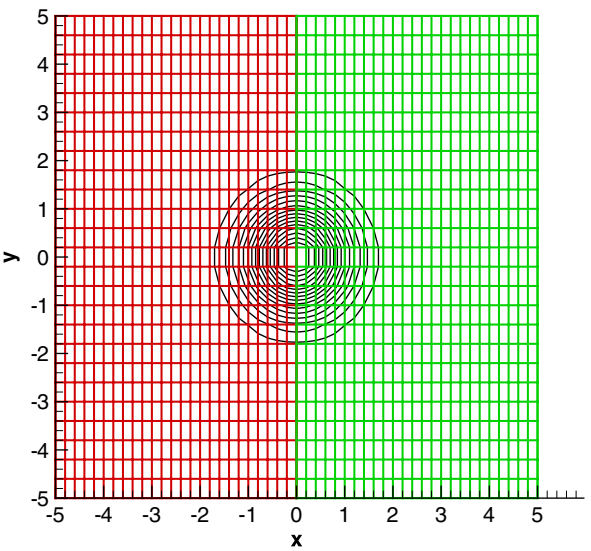

Figure 6. Matching boundaries—Yee vortex.

the coarse, medium and fine grid, respectively. Fourth-order linear coefficient of artificial viscosity is chosen equal to $\frac{1}{12}$. There is no addition of second-order non-linear artificial viscosity. For JST scheme, the computed accuracy orders (see Table I) are 2, 1.93 and 1.1, respectively, for uniform, stretched and irregular grids. As expected, the DNC formulation provides an order of accuracy of 3 on regular Cartesian meshes. We observe also that on an irregular Cartesian mesh, the order of accuracy is reduced to 1 if the schemes are not weighted by the distances. On the other hand, FVW-3 scheme is third-order accurate on all Cartesian meshes.

The finite-volume schemes have also been applied on curvilinear meshes (see Table II) and the impact of the weighted discretization operators is measured. If the mesh is really stretched, Table II shows that orders of accuracy of JST and FV-3 schemes are found to be 1. On the contrary, FVW-3 scheme produces a lower error and order of accuracy is close to 2.4, in good agreement with the theory.

DOI: 10.1002/fld

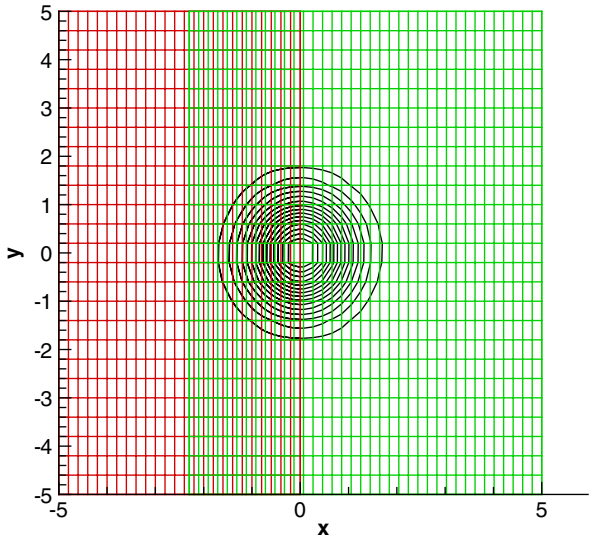

Figure 7. Non-matching boundaries (chimera)—Yee vortex.

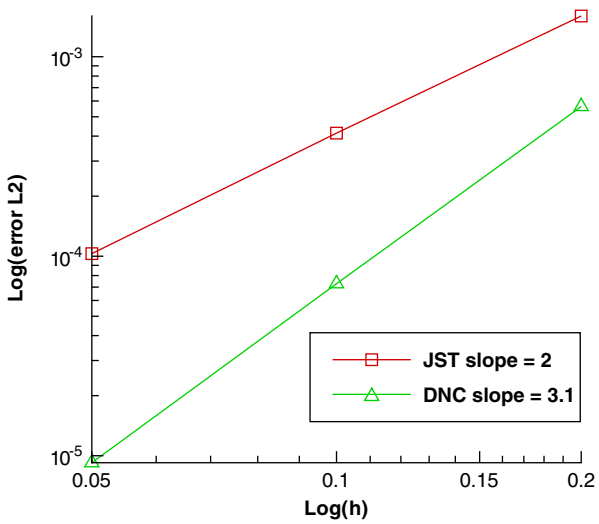

Figure 8. Accuracy study with matching boundaries—Yee vortex.

4.1.2. Overlapping Cartesian meshes. We now consider a domain with two overlapping Cartesian regular meshes. Parameters of artificial viscosity are identical to the single mesh study. When boundaries between the two meshes are matched (see Figure 6), interpolations should be exact and only numerical scheme error should occur. Practically, the order of accuracy (see Figure 8) is found out to be the same as in a single block mesh. In the case of non-matching boundaries (see Figure 7), the order of interpolation accuracy is important. As expected, for these chimera

DOI: 10.1002/fld

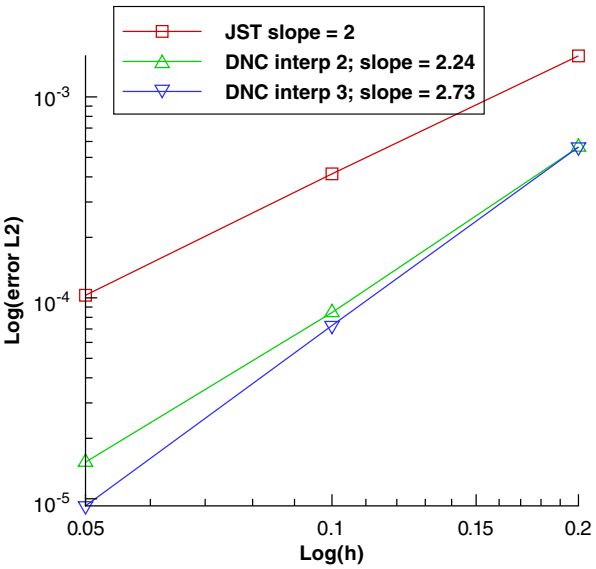

Figure 9. Accuracy study with non-matching boundaries (chimera)—Yee vortex.

boundaries, the computed order of accuracy of DNC formulation is close to three only with third-order interpolation (Figure 9).

4.2. Subsonic flow over an NACA0012 airfoil

In the present section, an inviscid flow over the NACA0012 airfoil at Mach number $M_\infty = 0.63$ and angle of attack $\alpha = 2°$ is considered. Schemes corresponding to fluxes (8) and (11) are used with the simple volume integral approximation (13), since they give, as expected, the same results when used with approximation (18) of the volume integral for steady cases. Linear fourth-order dissipation coefficient is chosen equal to $\frac{1}{12}$, there is no addition of second-order non-linear artificial viscosity for all the computations and Courant–Friedrichs–Lewy (CFL) number is equal to 1000.

4.2.1. Single block curvilinear meshes. The accuracy of schemes is first investigated in a computational domain made of single block curvilinear meshes of C topology. Three meshes of increasing density are considered with 69×11, 138×22 and 276×44 cells, respectively. In each grid, far-field boundary is located at 20 chords from the airfoil. The finest mesh is partly represented in Figure 10. As far as conservative variables are checked, quite similar solutions are obtained on each grid with JST, FV-3 and FVW-3 schemes.

Typical solution on the fine grid is represented in Figure 11. The entropy error $\sum$, which is a very sensitive flow quantity is considered here to evaluate the accuracy of schemes. It is computed by the following formula:

$$\sum = \frac{s - s_\infty}{s_\infty} \tag{46}$$

DOI: 10.1002/fld

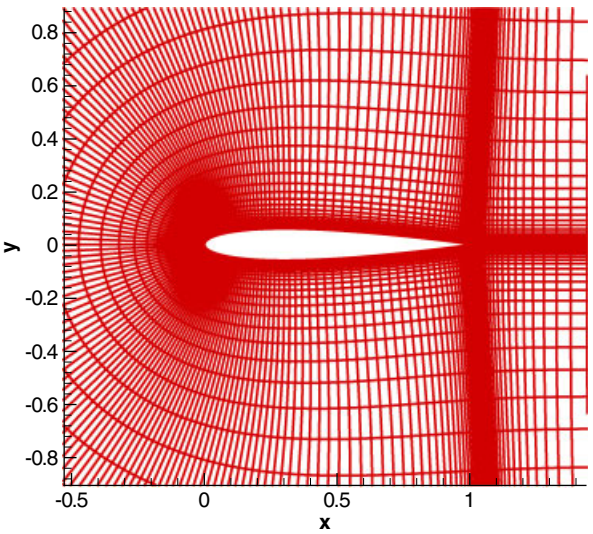

Figure 10. C-Grid 276×44 cells for NACA0012 airfoil, partial view.

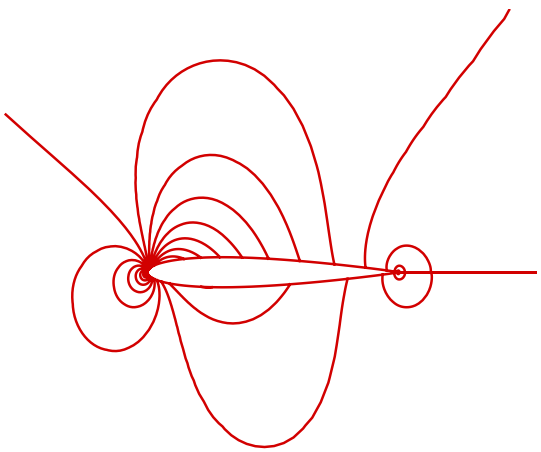

Figure 11. Density lines with FVW-3 scheme (276×44).

where $s = p/\rho^{\gamma}$ is an exponential of the entropy and s_{∞} the same quantity at infinity. In Figures 12–14, the entropy error on the airfoil surface computed for each grid, respectively, in the case of JST, FV-3 and FVW-3 schemes is plotted. We can observe that FV-3 and FVW-3 schemes give better result than JST scheme. Finally, the accuracy of schemes is evaluated from the L^2 norm of entropy error in Figure 15. The weighted third-order scheme FVW-3 provides an accuracy order which is close to 2.3, while the JST classical scheme is only 1.6 order accurate.

DOI: 10.1002/fld

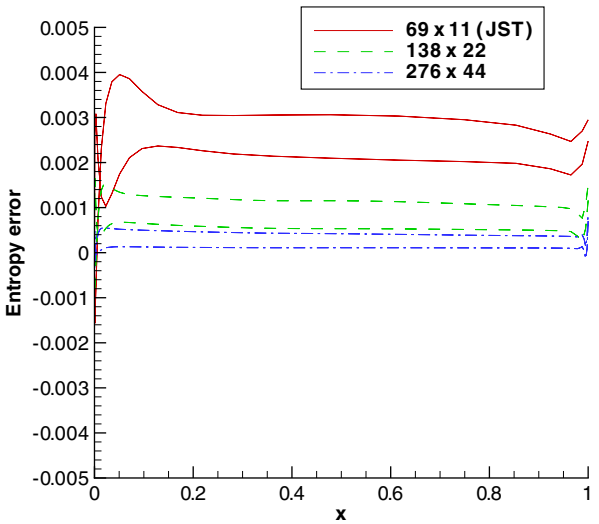

Figure 12. Entropy error at the wall for JST scheme on different meshes for NACA0012 airfoil.

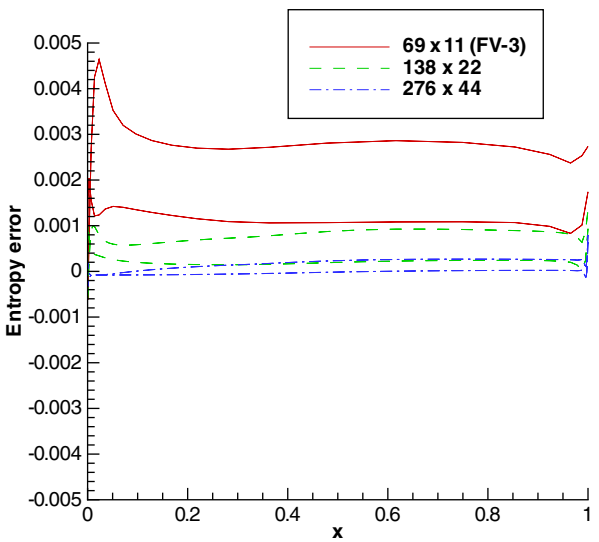

Figure 13. Entropy error at the wall for FV-3 scheme on different meshes for NACA0012 airfoil.

4.2.2. Automatic mesh Cartesian generation. No adaptation to the solution. JST and third-order method are now compared on a composite curvilinear/Cartesian computational set of grids. On regular Cartesian grids, the DNC formulation is favored for efficiency reasons. Consequently, the third-order method corresponds to the coupling between DNC formulation on Cartesian grids and FVW-3 scheme on body curvilinear mesh. For this computation, a body mesh of 201×14 cells is extracted from the fine single block mesh (276×44). Initial background mesh (see Figure 16)

DOI: 10.1002/fld

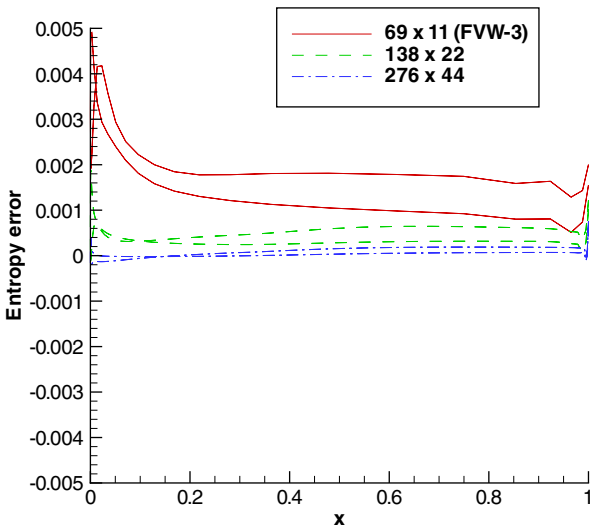

Figure 14. Entropy error at the wall for FVW-3 scheme on different meshes for NACA0012 airfoil.

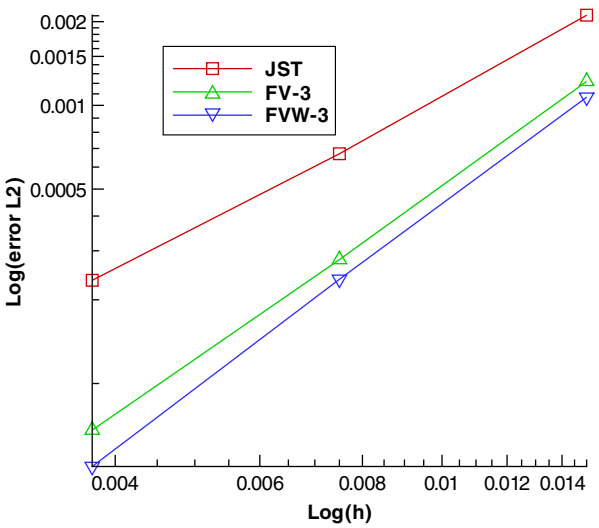

Figure 15. Accuracy order for JST, FV-3 and FVW-3 schemes for NACA0012 airfoil.

consists of isotropic Cartesian grids, with overlap, generated automatically. The space increment of the first Cartesian grid is chosen purposefully large and the mesh globally contains 30 000 points.

The solution and the convergence history with the third-order scheme are shown, respectively, in Figures 17 and 18. The results show that JST and third-order schemes produce a significant entropy error at the wall (Figures 19 and 20), in particular near the leading edge and trailing edge regions. As a matter of fact, error made in Cartesian grid propagates up to the wall.

DOI: 10.1002/fld

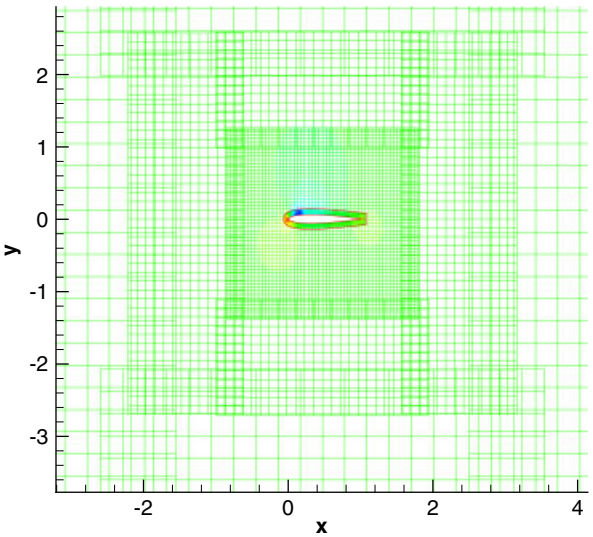

Figure 16. Chimera mesh without adaptation, partial view.

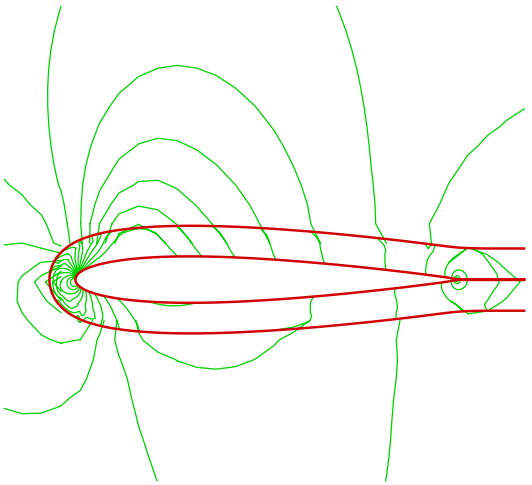

Figure 17. Density lines with DNC/FVW-3 method for chimera mesh.

4.2.3. Automatic Cartesian mesh adaptation. In a second step, adaptation to the solution is performed using refinement indicator based on the gradient of Mach number. Five remeshings are made. Mesh is adapted to the numerical solution every 400 iterations, the first remeshing being done after 400 iterations. The number of points is increased by a growing factor $\alpha = 1.25$ for the five remeshings. Results are given after 5000 iterations and the convergence history of the computation is plotted in Figure 21. The peaks that are observed are due to remeshings. They correspond to interpolation of the solution on the new generated mesh from solution of the preceding mesh.

DOI: 10.1002/fld

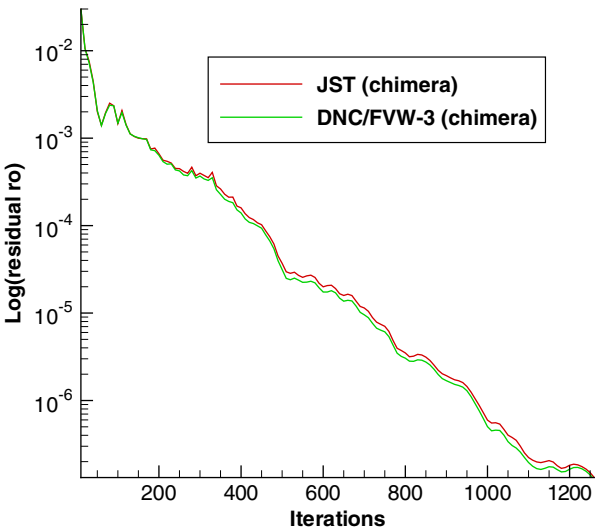

Figure 18. Convergence history (CFL = 1000) on chimera mesh.

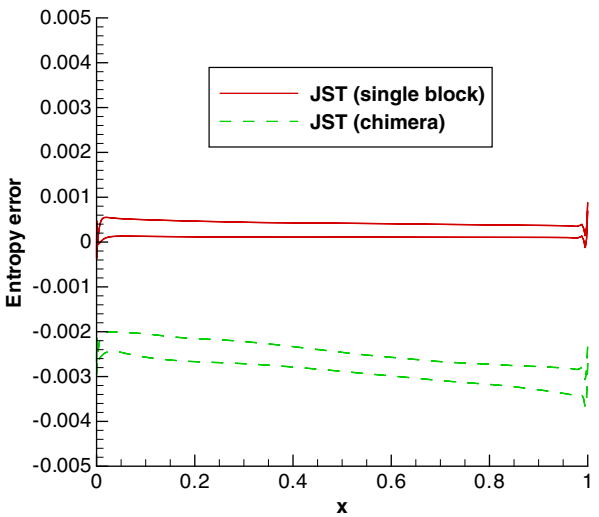

Figure 19. Entropy error at the wall for JST method on the fine single block mesh and on the chimera mesh.

Figure 22 shows that the mesh is refined in the vicinity of the leading edge and trailing edge and the solution is shown in Figure 23. We observe in Figures 24 and 25 that adaptation allows to reduce errors by a large amount in these regions. For JST and DNC/FVW-3 methods, entropy error is comparable to error on single block mesh.

DOI: 10.1002/fld

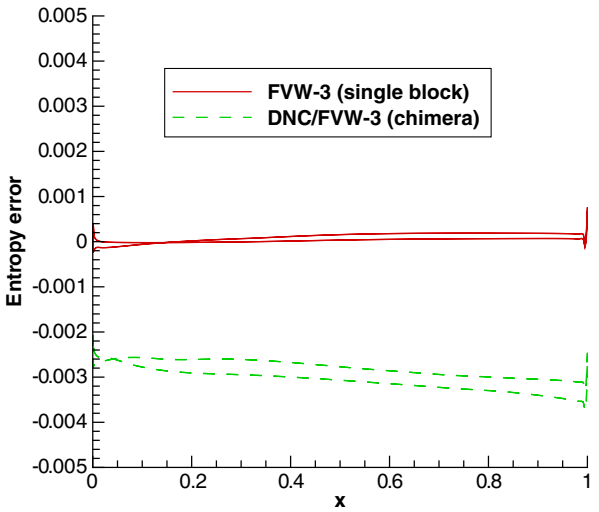

Figure 20. Entropy error at the wall for FVW-3 scheme on the single block mesh and for DNC/FVW-3 on the chimera mesh.

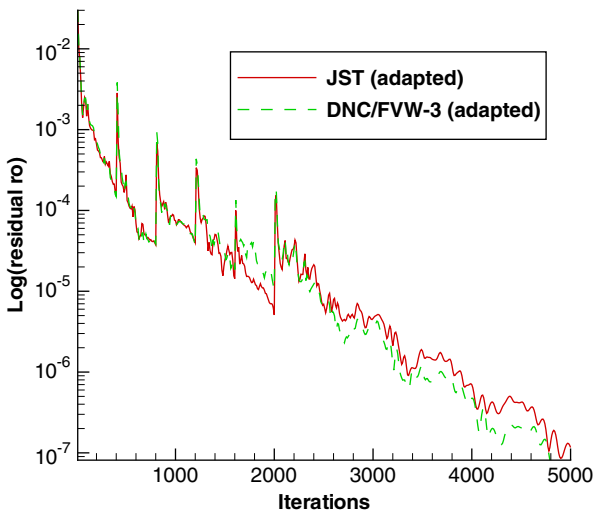

Figure 21. Convergence history (CFL = 1000) with adaptation.

4.3. Inviscid flow around a hovering helicopter blade

The third-order mesh adaptation technique is applied now to the computation of the inviscid flow around an isolated blade of the ONERA 7*A* helicopter rotor in hover. The Cartesian topology is not very well adapted to the calculation around a hovering rotor. It is more judicious to choose a cylindrical topology as in the work of Canonne *et al*. [14], which also uses an automatic mesh adaptation technique. However, the Cartesian mesh adaptation is more general and should also be

DOI: 10.1002/fld

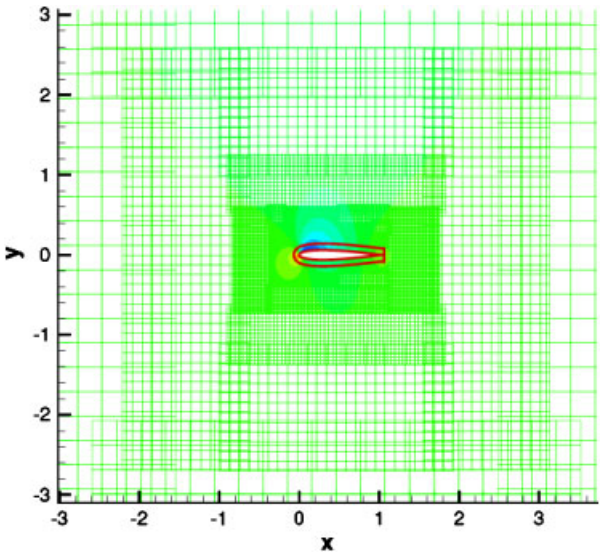

Figure 22. Partial view of chimera mesh after five remeshings of Cartesian adaptation.

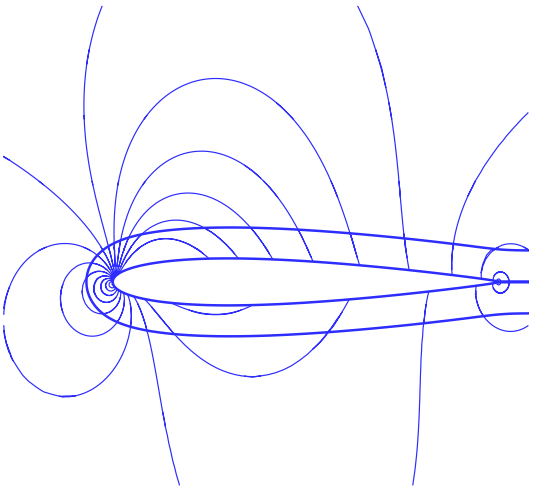

Figure 23. Density lines with DNC/FVW-3 method on the adapted mesh.

applied to rotor in forward flight. The aim of this section is to capture accurately the vortex emitted at the blade tip and to show the possible improvements by comparing the results obtained with the JST method. The 3-D compressible Euler equations are solved in a blade-attached rotating reference frame. The flight conditions correspond to tip Mach number $M_{\text{tip}} = 0.662$ and a collective pitch angle $\Theta_c = 7.5°$. The first computation is performed with automatic mesh generation and the second using automatic mesh adaptation technique. For the third-order numerical scheme, it was decided to apply the FV-3 scheme on the blade mesh. Indeed, it has been shown, in the calculation

DOI: 10.1002/fld

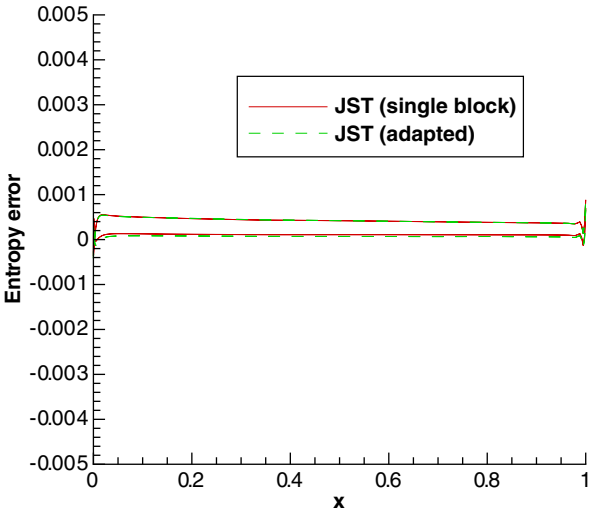

Figure 24. Entropy error at the wall for JST method on the single block fine mesh and on the adapted mesh.

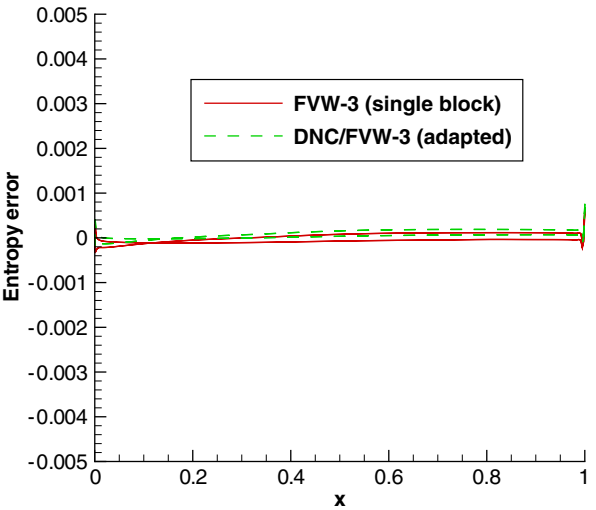

Figure 25. Entropy error at the wall for FVW-3 scheme on single block mesh and for DNC/FVW-3 method on the adapted mesh.

of the previous test case for the NACA0012 airfoil, that for a regular mesh, it was possible to obtain an accurate solution without using weighted extension.

The equations are advanced in time using a backward Euler scheme with factorized LU implicit stage [11] and the CFL number is chosen equal to 15. Finally, linear fourth-order dissipation coefficient is chosen equal to $\frac{1}{12}$ on blade mesh and equal to 0.014 on Cartesian mesh. Furthermore, there is no addition of second-order non-linear artificial viscosity.

DOI: 10.1002/fld

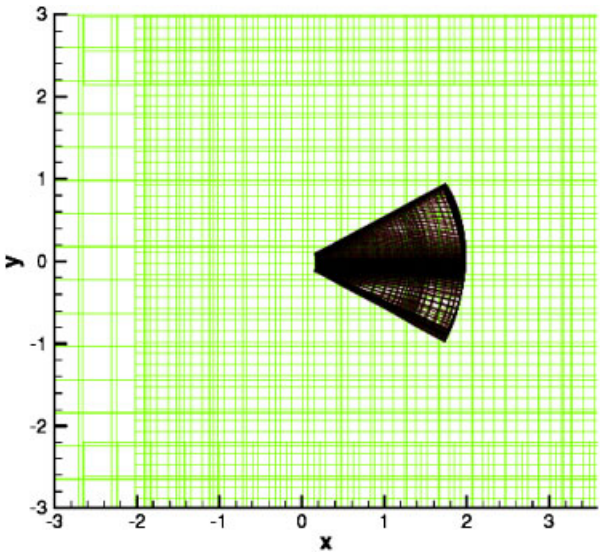

Figure 26. Chimera mesh without adaptation.

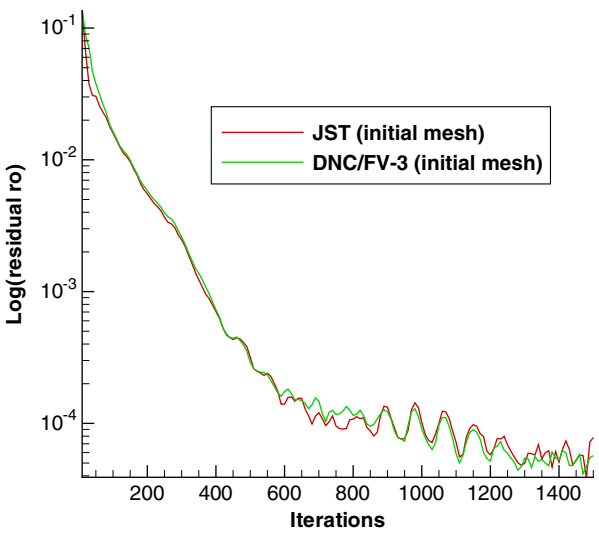

Figure 27. Convergence history on initial mesh, CFL = 15.

4.3.1. Automatic Cartesian mesh generation. No adaptation to the solution. As a preliminary step, the automatic mesh generation is used to generate the background mesh. The mesh of the blade is made of $140 \times 26 \times 17$ cells. The minimal number of points of Cartesian grids in each direction is set to 6 points. The step factor between two consecutive grids is chosen equal to 3. With these parameters, the procedure generates 140 000 points in seven Cartesian blocks. The initial mesh

DOI: 10.1002/fld

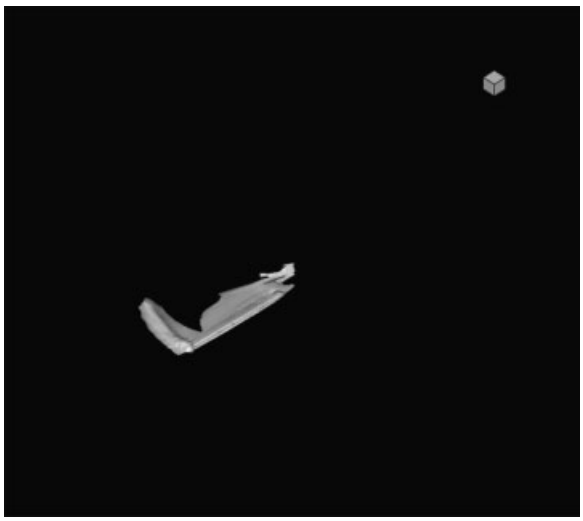

Figure 28. Vorticity iso-surface on the initial mesh.

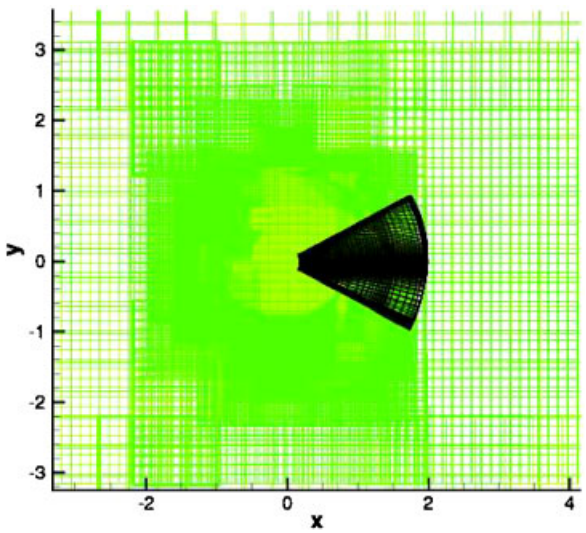

Figure 29. Partial view of Cartesian mesh after 10 remeshings.

is shown in Figure 26. In Figure 27, the convergence histories of the second- and third-order schemes are similar. After 1500 iterations, the residual is decreased by four orders. When looking to the iso-vorticity surface ($\|\text{curl}\, V\| = 0.8$) in Figure 28, one can notice that the tip vortex is not captured and the wake is strongly dissipated. Moreover, the results are similar with third-order scheme. The results obtained on this mesh are used to initialize JST and third-order (DNC/FV-3) mesh adaptation methods.

DOI: 10.1002/fld

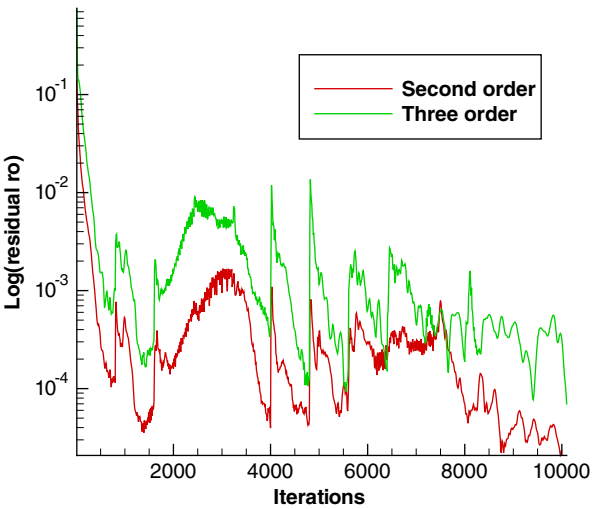

Figure 30. Convergence history with adaptation, CFL = 15.

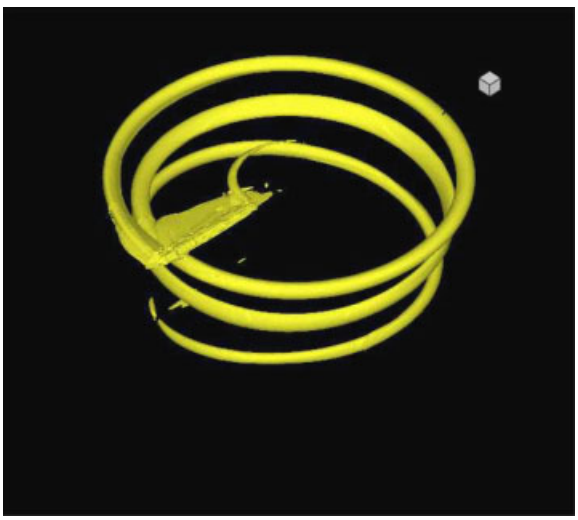

Figure 31. Vorticity iso-surface on the adapted mesh (JST method).

4.3.2. Automatic Cartesian mesh adaptation. For the second calculation of the rotor in hover, the mesh is adapted to the numerical solution and the refinement indicator is the modulus of the vorticity, i.e. of the curl of the fluid velocity vector. First, 800 iterations are performed on the initial mesh; then the Cartesian grids are adapted every 800 iterations. For this computation, 10 remeshings are realized. The remeshing frequency is chosen sufficiently big in order to improve the convergence between the remeshings and consequently enable to obtain a more accurate solution. The number of points is increased by a growing factor equal to 1.4 at each remeshing. The number

DOI: 10.1002/fld

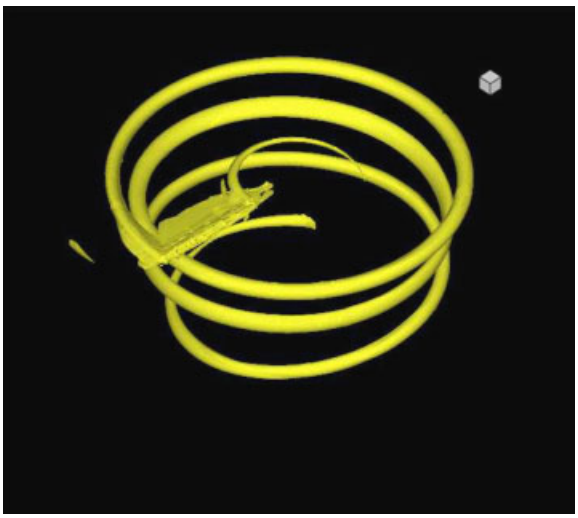

Figure 32. Vorticity iso-surface on the adapted mesh (DNC/FV-3 method).

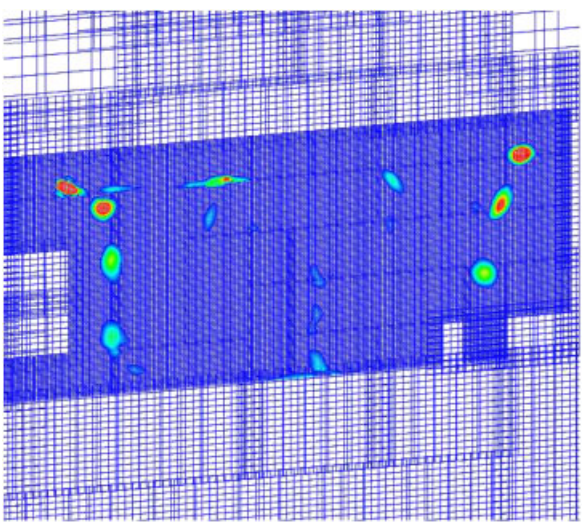

Figure 33. Vorticity contour at slices 20° in the blade wake on the adapted mesh (JST method).

of points in the last mesh is approximately 7 millions with the second- and third-order methods and number of blocks is equal to 165 with JST method and equal to 163 with third-order method. The adapted mesh is displayed in Figure 29 and results are given after 10 000 iterations. The convergence history of the calculation is plotted in Figure 30. In this figure, we observe the peaks caused by remeshings as in the case of NACA0012 airfoil test case. The residual is decreased approximatively by four orders for JST and third-order methods after 10 000 iterations.

DOI: 10.1002/fld

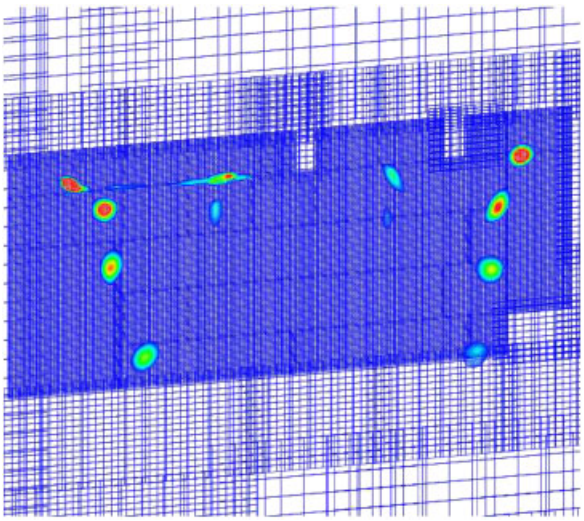

Figure 34. Vorticity contour at slices 20° in the blade wake on the adapted mesh (DNC/FV-3 method).

The different iso-vorticity surfaces in Figures 31 and 32 show that the tip vortex is much better captured and less dissipated than in the previous computation. This fact can be explained by the higher number of mesh points and their greater concentration in the vortex area. The vortex can be followed for approximately 1080° of age by using JST method. The third-order method allows to improve this result slightly; it is possible to follow it for approximately 1150° of age. Besides, the blade's root is better represented by using the third-order method. The vorticity contours for computations realized with the third-order method (Figure 34) show that the vortices are more intense even if the difference with the second-order method (Figure 33) is less significant. Besides, position of vortices are different with third-order method because it allows to reduce dispersive error. Finally, CPU time required for the computation with third-order method is only 3% superior to CPU time with JST method. Consequently, these CPU times are quite similar for the two calculations.

5. CONCLUSION

A third-order mesh adaptation method has been developed successfully for solving Euler equations. We have shown on basic 2-D test cases that chimera method with automatic mesh generation and adaptation method can be coupled with third-order numerical schemes enough to achieve a global accuracy comparable to single block meshes. Moreover, the third-order mesh adaptation technique has been extended to 3-D Euler equations. The computations of the isolated blade in hover have shown that the third-order numerical scheme allows to improve the results at a very low cost in CPU time. Future work will be devoted to further increase the accuracy order of the numerical scheme on Cartesian grids to improve the wake capture.

DOI: 10.1002/fld

REFERENCES

1. Steger J, Dougherty F, Benek J. A chimera grid scheme. In *Advances in Grid Generation*, Ghia KN, Chia U (eds); *ASME FED*, vol. 5, 1983; 59–69.
2. Meakin RL. An efficient means of adaptive refinement within systems of overset grids. *Twelfth AIAA Fluid Dynamics Conference*, San Diego, California, 1995; 844–857, *AIAA Paper 95-1722-CP*.
3. Benoit C, Jeanfaivre G. Three dimensional inviscid isolated rotor calculations using chimera and automatic Cartesian partitioning methods. *Journal of the American Helicopter Society* 2003; **48**:128–138.
4. Jameson A, Schmidt W, Turkel E. Numerical solutions of the Euler equations by finite volume methods using Runge–Kutta time stepping. *AIAA Paper 81-1259*, 1981.
5. *CFD Higher Order Discretization Methods*. VKI LS 2006-01, 2006.
6. Cinnella P, Lerat A. A study of turbulent compressible flows over oscillating airfoils using a high-order accurate numerical scheme. *Computational Fluid Dynamics Journal* 2000; **9**:90–104.
7. Rezgui A, Cinnella P, Lerat A. Third-order accurate finite volume schemes for Euler computations on curvilinear meshes. *Computers and Fluids* 2001; **30**:875–901.
8. Sherer SE, Scott JN. High-order compact finite-difference methods on general overset grids. *Journal of Computational Physics* 2005; **210**:459–496.
9. Chesshire G, Henshaw W. Composite overlapping meshes for the solution of partial differential equations. *Journal of Computational Physics* 1990; **90**:1–64.
10. Cinnella P. Simulation d'écoulements compressibles turbulents autour de profils oscillants par une méthode numérique de haute precision. *Ph.D. Thesis*, Ecole Nationale Superieure d'Arts et Metiers, Paris, 1999.
11. Peter J, Drullion F. Large stencil viscous flux linearization for the simulation of 3D compressible turbulent flows with backward-Euler schemes. *Computers and Fluids* 2007; **36**:1005–1027.
12. Jeanfaivre G, Benoit C, Le Pape MC. Improvement of the robustness of the chimera method. *Thirty-second AIAA Fluid Dynamics Conference*, Saint Louis, Missouri, June 2002; *AIAA Paper 2002-3290*.
13. Yee HC, Sandham ND, Djomehri MJ. Low-dissipative high-order shock-capturing methods using characteristic-based filters. *Journal of Computational Physics* 1999; **150**:199–238.
14. Canonne E, Benoit C, Jeanfaivre G. Cylindrical mesh adaptation for isolated rotors in hover. *Aerospace Science and Technology* 2004; **8**(1):1–10.

DOI: 10.1002/fld